Reverse time migration approaches for DAS VSP

Jorge E. Monsegny, Daniel Trad and Don C. Lawton

ABSTRACT

Distributed acoustic sensing is a promising technology for seismic monitoring that uses optical fibre as a sensing element instead of geophones. In contrast to geophones, it produces a signal proportional to the strain, or strain rate depending on the vendor, instead of particle velocity. To apply processing techniques, like migration, this strain is usually transformed to particle velocity beforehand. We perform the migration directly in the strain and an associated pressure domains by modifying the wave equation. We compare its results on the reflectivity by using a synthetic model and also compare the migration results with data from the Containment and Monitoring Institute Field Research Station. In the synthetic example we obtained a good match between the migrated amplitudes at the reflector depth and the theoretical reflection coefficients. The real data migrations showed a quality similar to the usual path of transforming to vertical particle velocity before migration.

INTRODUCTION

The Containment and Monitoring Institute Field Research Station, CAM-FR'S, is a research facility where up to 400 tonnes of CO_2 are being injected annually within a 5 year plan (Lawton et al., 2015; Macquet et al., 2019). It is located near Brooks, Alberta, Canada. In order to monitor the injected CO_2 a variety of monitoring technologies are being used there (Lawton et al., 2017).

Distributed acoustic sensing, DAS, is one of those technologies (Mateeva et al., 2013). It consists of an optical fibre used as the sensing element instead of geophones, and an interrogator device that sends light pulses to the fibre and measures the strain or strain rate produced by seismic waves perturbing the fibre from the backscattered light (Hartog, 2018). At CaMI-FRS, a 5km loop of fibre is permanently installed. Part of that loop goes through two observation wells where it is used to record VSP seismic data.

Reverse time migration, RTM, is commonly used to create an image of the subsurface using seismic data (Baysal et al., 1983). It has been used to monitor the injection of CO_2 using conventional geophone VSP data (Wang et al., 2011). As DAS measures strain, or strain rate, there must be a transformation from DAS to geophone data before performing the RTM. Two usual transformations are Bóna et al. (2017) and Daley et al. (2016).

The geophone response to P-waves is the sine of the wave angle of propagation while the DAS response is $\sin^2$. (Benioff, 1935). This means that a geophone is able to tell the difference between two waves travelling in different directions parallel to its axis while DAS is not. This difference can be important in VSP data that has upgoing and downgoing wavefields. In this sense, the response of DAS is more akin to a hydrophone, that measures pressure.
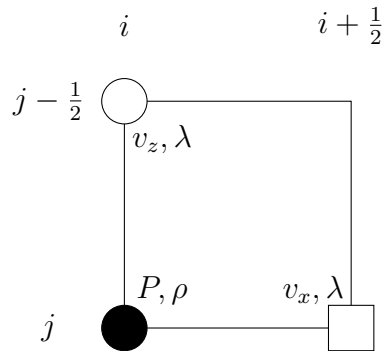
FIG. 1. Location of the finite difference wavefields in the staggered grid. Pressure P and density ρ are at integer coordinates (i, j), vertical particle velocity v_z is at coordinates $(i, j - 1/2)$, horizontal particle velocity v_x is at $(i+1/2, j)$ and Lamé parameter λ is defined at both $(i, j-1/2)$ and $(i+1/2, j)$

We perform RTM with DAS data, without transforming it to geophone data, in the strain and pressure domains and compare the results with the usual RTM of geophone data. We find that these two migrations offer a response more proportional to the theoretical reflection coefficients than the particle velocity migration.

In the first part we describe the modified wave equation systems and the imaging conditions of the pressure and strain migrations. In the second part we use a synthetic model to ascertain the pressure and strain migrations quality by comparing their results with the theoretical reflection coefficients. Finally, in the last part, we perform the pressure and strain migrations using walkaway VSP DAS data from CaMI-FRS.

METHODS

To derive the strain domain and pressure domain RTM for DAS data, we use a staggered acoustic finite difference system in pressure P and particle velocities v_x and v_z (Liang et al., 2018):

$$
\begin{aligned}
\frac{\partial P}{\partial t} &= \lambda \left(\frac{\partial v_x}{\partial x} + \frac{\partial v_z}{\partial z} \right) + s \\
\frac{\partial v_x}{\partial t} &= \frac{1}{\rho} \frac{\partial P}{\partial x} \\
\frac{\partial v_z}{\partial t} &= \frac{1}{\rho} \frac{\partial P}{\partial z},
\end{aligned}
\tag{1}
$$

where the medium properties are density ρ and Lamé parameter λ. The source, s, excites the pressure equation. Figure 1 shows the locations in the staggered grid of the wavefields in the system of equations 1.

To link pressure and strain rate, what DAS measures, we use the following identities. In an acoustic medium, the pressure P is related to the normal stresses:

$$-P \;=\; \sigma_{xx} = \sigma_{yy} = \sigma_{zz}, \tag{2}$$

while all the shear stresses are zero. In a similar fashion, the normal strains are equal to each other, $\epsilon_{xx} = \epsilon_{yy} = \epsilon_{zz}$, while the shear strains are also zero. Using this, there is a relationship between pressure and normal strain:

$$
\begin{aligned}
-P \;&=\; \sigma_{zz} \\
&=\; \lambda(\epsilon_{xx} + \epsilon_{yy} + \epsilon_{zz}) + 2\mu\epsilon_{zz} \\
&=\; 3\lambda\epsilon_{zz}
\end{aligned}
\tag{3}
$$

Pressure RTM for DAS

The first RTM transforms the DAS input seismograms from strain rate, $f = \frac{\partial \epsilon_{zz}}{\partial t}$, to pressure using equation 3:

$$
\begin{aligned}
P \;&=\; -3\lambda\epsilon_{zz} \\
&=\; -3\lambda \int \frac{\partial \epsilon_{zz}}{\partial t} dt \\
&=\; -3\lambda \int f\, dt.
\end{aligned}
\tag{4}
$$

In the practice, the integration produces undesirable very low frequencies that we need to filter after this transformation. We apply a 5Hz high pass filter in order to do this.

The RTM migration forward and backward propagations are carried out using the finite difference system of equation 1 with the transformed to pressure seismograms in the backward propagation part.

The imaging condition is the cross-correlation of forward, P^f, and backward, P^b, pressure wavefields, normalized by the source illumination to diminish migration artifacts and obtain a dimensionless result:

$$I_P(x) \;=\; \int_0^{t_{max}} \frac{P^f(x)P^b(x)}{P^f(x)P^f(x)^*} dt, \tag{5}$$

Strain RTM for DAS

Instead of transforming the DAS seismograms to pressure, we can introduce equation 3 in the finite difference system of equation 1 to obtain a system in strain and particle velocity:

$$
\begin{aligned}
\frac{\partial \epsilon_{zz}}{\partial t} &= -\frac{1}{3}\left(\frac{\partial v_x}{\partial x} + \frac{\partial v_z}{\partial z}\right) - \frac{s}{3\lambda} \\
\frac{\partial v_x}{\partial t} &= -3\frac{1}{\rho}\frac{\partial(\lambda\epsilon_{zz})}{\partial x} \\
\frac{\partial v_z}{\partial t} &= -3\frac{1}{\rho}\frac{\partial(\lambda\epsilon_{zz})}{\partial z},
\end{aligned}
\tag{6}
$$

where the locations of each wavefield in the staggered grid is the same as in Figure 1 with ϵ_{zz} in the place of P.

In this system, we have to calculate spatial derivatives of the product $\lambda\epsilon_{zz}$. Apart from the additional computational overhead of doing these derivatives, we have to be careful with the discontinuities of λ that can yield immeasurable derivatives and make unstable the system. We use instead a smoothed version of λ to avoid this possibility.

The second RTM starts by turn the DAS seismograms into strain by time integration and filtering of very low frequencies as described earlier. Similar to the previous RTM, the forward and backward propagations are carried out using the finite difference system of equation 6 using the transformed to strain seismograms in the backward propagation part.

In this case, the imaging condition is the cross-correlation of forward, ϵ_{zz}^f, and backward, ϵ_{zz}^b, strain wavefields. Again, we normalize by the source illumination to mitigate migration artifacts and obtain a dimensionless result:

$$
I_{\epsilon_{zz}}(x) = \int_0^{t_{max}} \frac{\epsilon_{zz}^f(x)\epsilon_{zz}^b(x)}{\epsilon_{zz}^f(x)\epsilon_{zz}^f(x)^*}dt,
\tag{7}
$$

SYNTHETIC TEST

We are going to do a synthetic experiment to test the response of the pressure and strain migrations showed in the previous section. For that, we are going to follow Chattopadhyay and McMechan (2008) where several imaging conditions are evaluated by migrating data from a two layered model and comparing the resulting migration image along the reflector with the theoretical reflectivities.

Figure 2 shows the velocity model we are going to use in the synthetic experiment. It has two layers and the velocities are close enough to provide a range of precritical reflection angles up to $77°$. On the other hand, the density model is constant so it does not influence the reflectivity values. With regard the survey, it is a single shot gather located at the top left corner of the model while the DAS fibre is located along the surface.
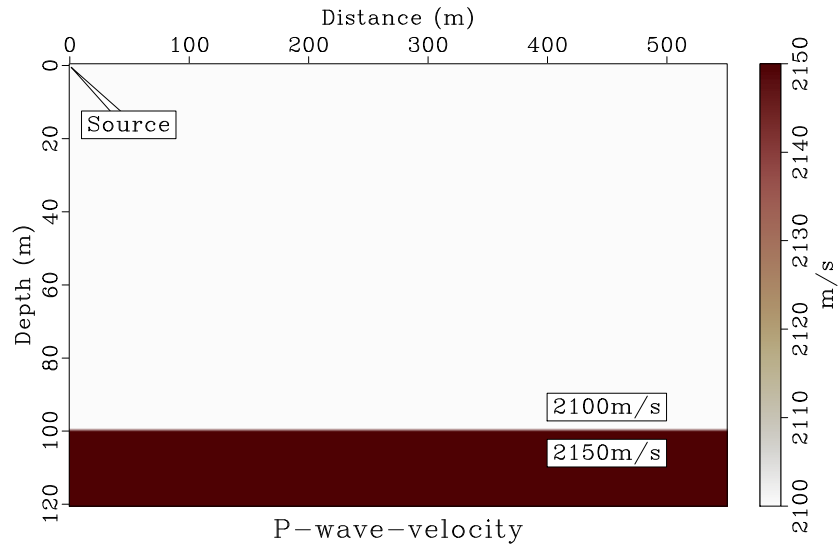
FIG. 2. Synthetic experiment velocity model. The velocities follow Chattopadhyay and McMechan (2008) to obtain a range of precritical reflection angles up to $77°$. The source is located at the top left corner and the DAS fibre along the surface.
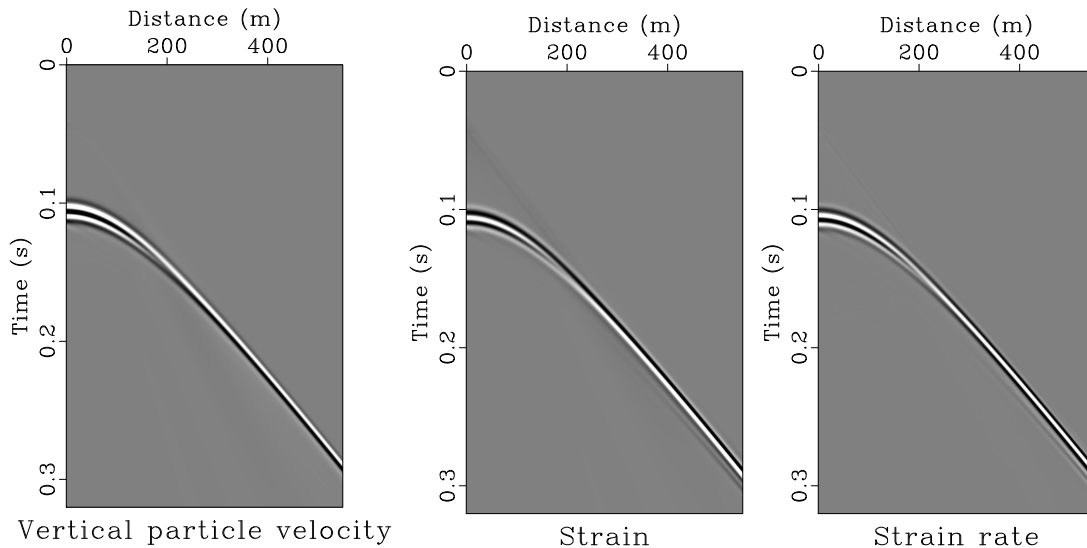

FIG. 3. Synthetic DAS gathers. They were generated by using a finite difference scheme based on the system of equations 6. On the left is the vertical particle velocity, v_z, and in the centre is the vertical strain ϵ_{zz}. The gather on the right is the strain rate and was created by deriving the gather on the middle. The first arrivals were muted.
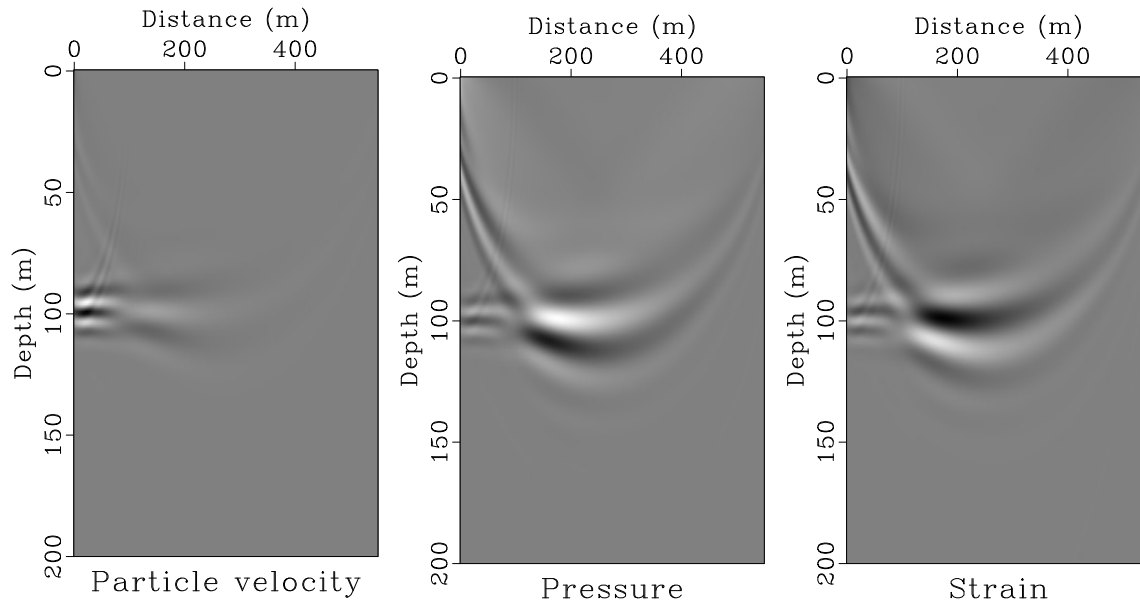
FIG. 4. Synthetic data RTM. On the left is the usual vertical particle velocity RTM. On the middle is the pressure RTM obtained by using the imaging condition of equation 5, while on the right is the strain RTM created by using the imaging condition in equation 7.

We generated the synthetic data using a finite difference system based on the system of equations 6 and recording the vertical particle velocity, v_z, and vertical strain, ϵ_{zz}, wavefields at the fibre locations. Figure 3 shows the vertical particle velocity gather on the left and the vertical strain on the middle. The strain rate gather on the right was generated by deriving the strain gather. The direct arrival was muted in all gathers.

The Figure 4 shows the migration results. On the left is the usual vertical particle velocity RTM when the data is from geophones. On the middle is the pressure RTM obtained as was explained in the previous section with the imaging condition of equation 5. On the right is the corresponding strain RTM, also explained in the previous section, with the imaging condition appearing in equation 7.

In Figure 5 we extracted the amplitudes of the RTM images of Figure 4 at 100m, the reflector depth. As we are interested in the relative amplitudes, we shifted and stretched these extracted amplitudes to match the theoretical geophone reflection coefficients also plotted on the images. These reflection coefficients were calculated with the usual expression for constant density:

$$R(\theta_1) = \frac{V_1 \cos(\theta_1) - V_2 \cos(\theta_2)}{V_1 \cos(\theta_1) + V_2 \cos(\theta_2)}, \tag{8}$$

where V_1 is the velocity of the top layer, V_2 the velocity of the bottom one, θ_1 is the incidence angle and θ_2 is the refraction angle that is related to θ_1 by Snell's law. In Figure 5,
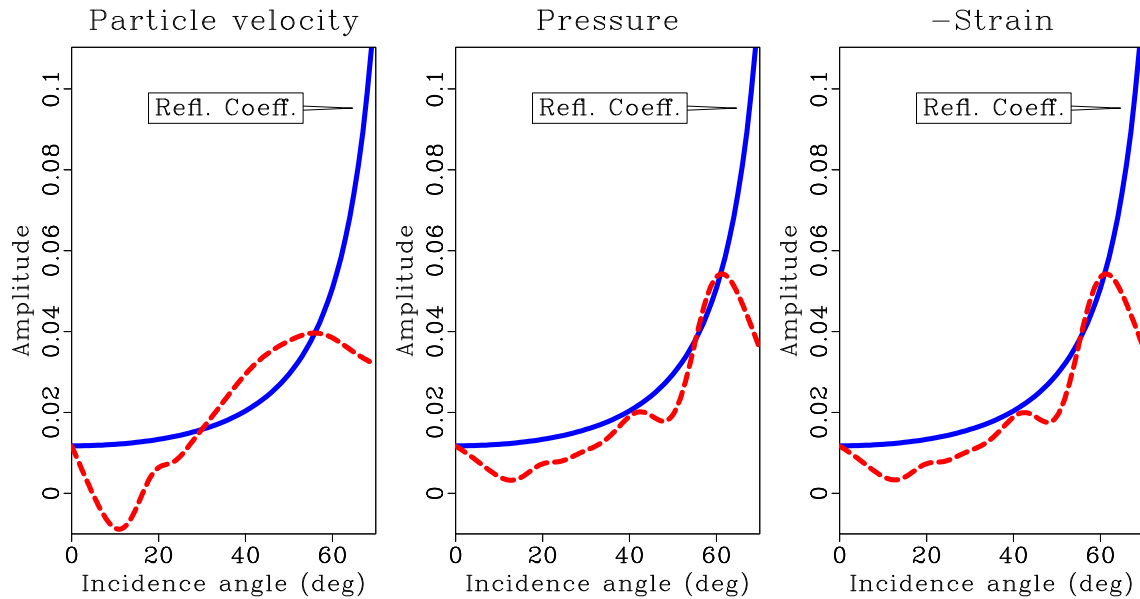
FIG. 5. Theoretical geophone reflectivity and amplitudes extracted from the RTM images of Figure 4 at the reflector depth, 100m. The extracted amplitudes were stretched and shifted vertically to match the theoretical curve. Note that we are plotting the extracted amplitude strain with opposite polarity.

notice that we plot the strain amplitude with the opposite polarity and that it is practically identical to the pressure amplitude plot.

FIELD DATA RTM

We also tested the pressure and strain migrations using real DAS data. The data is from a walkaway VSP survey acquired at CaMI-FRS. The Figure 6 displays a plan view showing the locations of the 17 shot points and the well location in the middle composing the survey. The nominal distance between shot points is 10m.

The profile view of the same figure shows the extension of the 300m DAS fibre inside the well. Only the data from the segment between 84m and 317m was used in the migrations due that data from other parts of the fibre were too contaminated with noise. The source was an Envirovibe with a linear sweep of 20s between 10 and 150Hz.

A subset of the 17 DAS VSP shot gathers appears in Figure 7. This data contains only the upgoing events and its processing consisted of geometry, first break picking, wavefield separation, gain for spherical transmission and loss, and deconvolution of the upgoing wavefield (Gordon, 2019).

The velocity and density models used in the migrations are in Figure 8. Both were scaled down from well log data and extended horizontally. The top 35m of the P-wave velocity model were obtained by a first arrivals tomography. The Lamé parameter λ, needed by the equation systems 1 and 6 was calculated from the acoustic approximation from the P-wave velocity V_p and the density ρ:
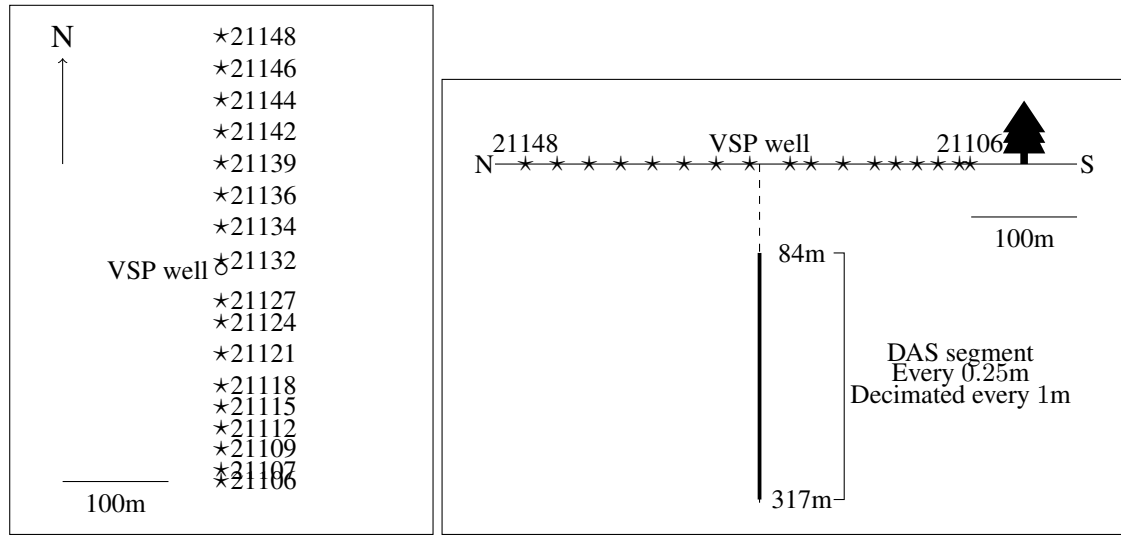
FIG. 6. Walkaway DAS VSP survey at CaMI-FRS. The plan view on the left shows the location of the 17 shot points with respect to the well in the middle. The distance between shot points is 10m in average. The profile view on the right shows the 300m of DAS fibre inside the well. We used data from the fibre segment between 87m and 317m due to its higher SNR.
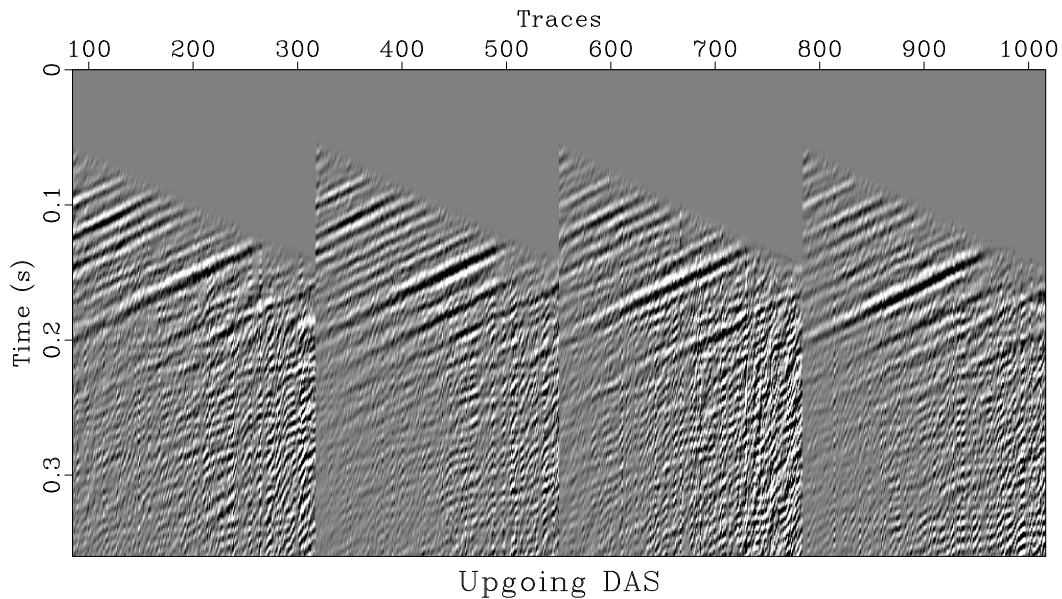

FIG. 7. Subset of the 17 DAS VSP shot gathers. This data is processed and contains only the upgoing events.
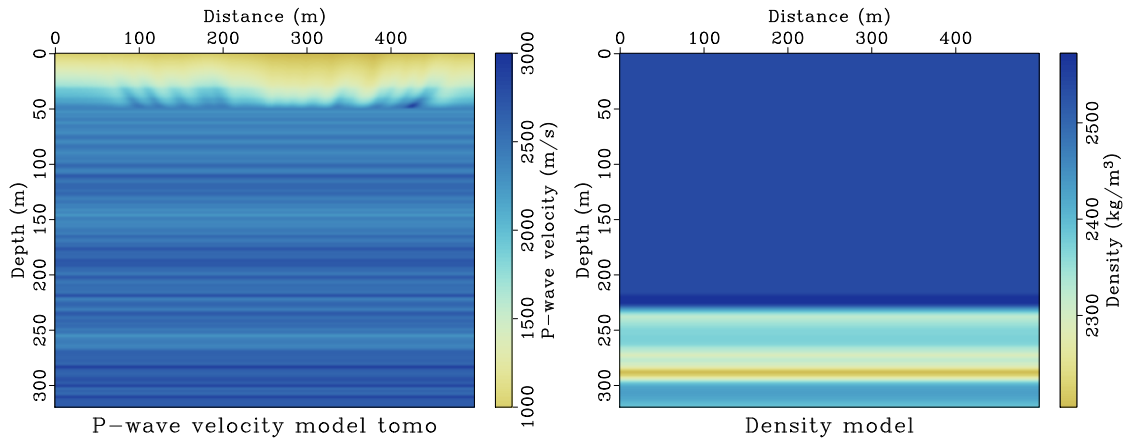
FIG. 8. P-wave velocity, left, and density, right, models used in the migrations. Both models were obtained from scaled down well log data, except the top 35m of the velocity model that was produced by a first arrivals tomography.
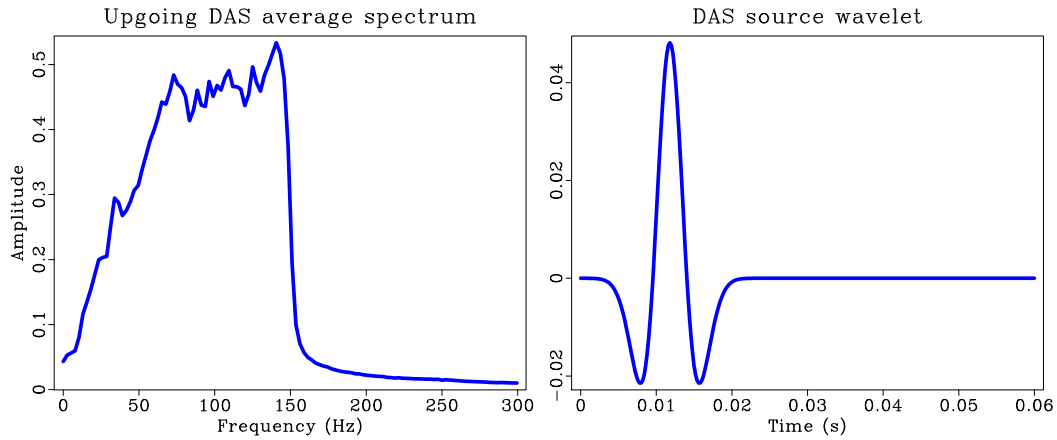

FIG. 9. The average upgoing average spectrum is on the left. It is mostly concentrated between 50 and 150Hz. The 100Hz Ricker wavelet used as source in the migrations is on the right.

$$\lambda = \rho V_p^2. \tag{9}$$

A spectral analysis of DAS data, shown in Figure 9, revealed that most of the frequencies are in a zone between 50Hz and 150Hz. For this reason a 100Hz Ricker wavelet, also shown in the same figure, is used as the source in the migrations as an approximation of a Klauder wavelet that is usually used in data produced by vibrational sources.

Finally, Figure 10 displays the reverse time migrations of the CaMI-FRS DAS VSP data. The top shows the usual RTM of DAS data that first transforms the data into vertical particle velocity using the method of Daley et al. (2016) and then performs a particle velocity RTM. In the middle is the pressure RTM for DAS data and in the bottom is the strain RTM for DAS data described before. The pressure and strain RTM images offer a similar quality than the usual RTM. Also, as noticed before in the synthetic example, Figure 5, the strain RTM has the opposite polarity of the pressure RTM.
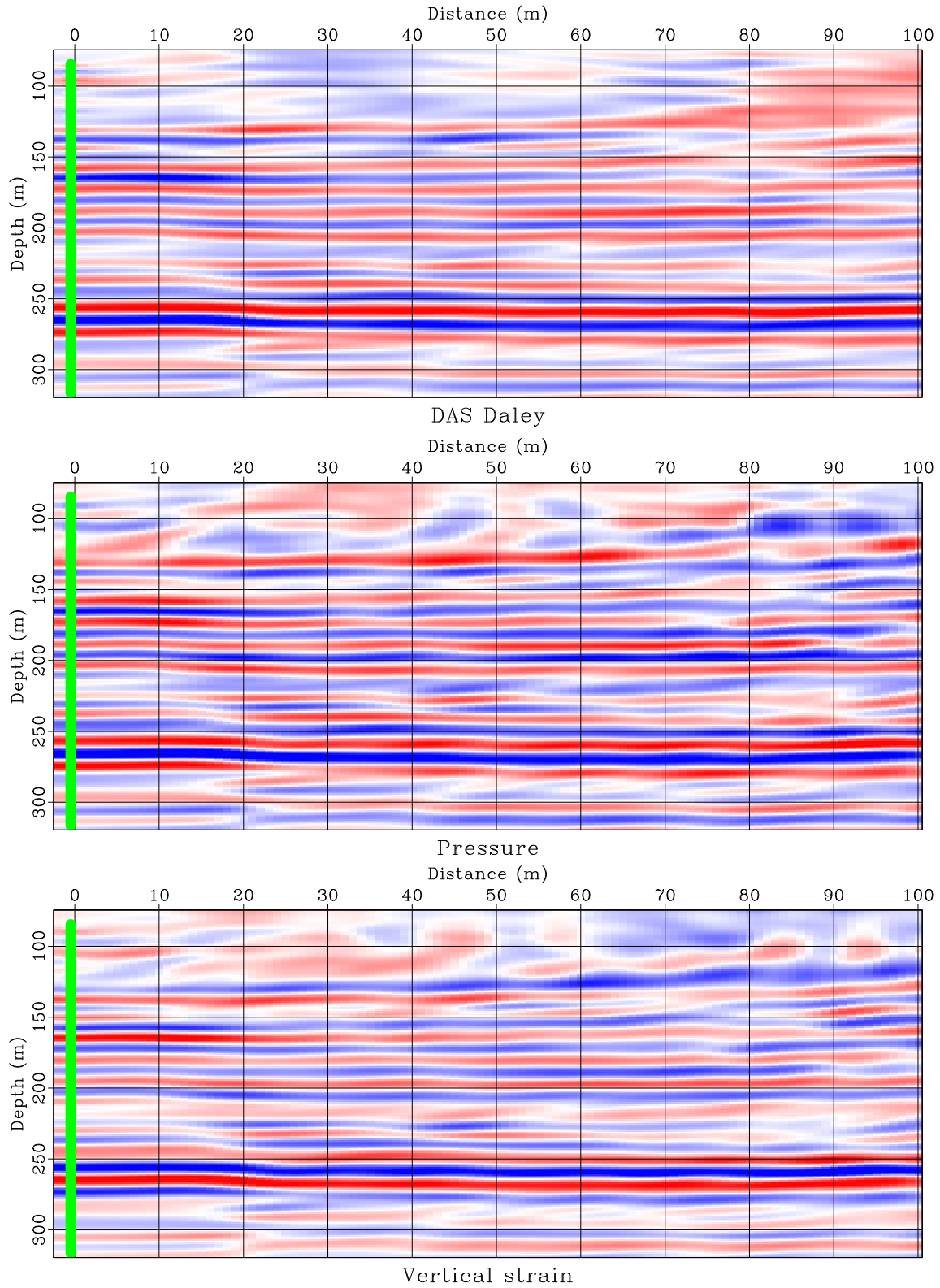
FIG. 10. VSP DAS migrations with data from CaMI-FRS. Top shows the usual workflow that first turns the DAS data into geophone data by using the method of Daley et al. (2016) and then preforms a particle velocity migration. Middle is the pressure RTM and bottom is the strain RTM.

DISCUSSION

Data from hydrophones, that measure pressure, is usually migrated using conventional methods. There is no need to transform them to a more geophone-like data. On the other hand, it seems that we have to transform the DAS data to particle velocity data before imaging. We wanted to create a RTM that worked directly in the kind of data measured by DAS or a related field, like pressure. The results from the synthetic and real data show that the imaging can be done without transforming the DAS data to geophone data.

In the synthetic test we scale the migrations amplitudes to match the theoretical reflectivities as we are interested in the relative values. We are after imaging techniques that preserve these relative values.

We used the Ricker wavelet shown in Figure 9 instead of a more normal Klauder wavelet calculated from the vibrational source sweep mainly because the Ricker wavelet looks like a smoothed version of the Klauder one.

The tomographic refinement of the shallow part of the velocity model helped to make more continuous reflectors, especially at the zone of interest between 250m and 300m. Other method that we tested was to apply static corrections, but the differences of elevations are of less than a metre. In addition, the enhanced velocity model is used during the forward and backward propagations. With the static corrections we would have to apply them to the forward propagated data before the imaging condition to match the backpropagated data.

CONCLUSIONS

Two reverse time migrations for strain and pressure data, more natural to DAS, data were developed.

The synthetic test showed that the relative amplitudes obtained with the strain and pressure migrations is similar to the theoretical reflectivities, so not only the kinematic behaviour of the reflectors can be produced but the dynamic one.

The real data test showed that the strain and pressure migrations have a similar quality to the migration of DAS data converted to particle velocity. This means that this kind of imaging can be done directly with DAS data without applying a transformation.

ACKNOWLEDGEMENTS

REFERENCES

Baysal, E., Kosloff, D. D., and Sherwood, J. W. C., 1983, Reverse time migration: GEOPHYSICS, **48**, No. 11, 1514–1524, `https://doi.org/10.1190/1.1441434`.

Benioff, H., 1935, A linear strain seismograph*: Bulletin of the Seismological Society of America, **25**, No. 4, 283–309, `https://pubs.geoscienceworld.org/bssa/article-pdf/25/4/283/2688655/BSSA0250040283.pdf`.

Bóna, A., Dean, T., Correa, J., Pevzner, R., Tertyshnikov, K., and Zaanen, L., 2017, Amplitude and phase response of DAS receivers, *in* 79th EAGE Conference and Exhibition 2017, `http://earthdoc.eage.org/publication/publicationdetails/?publication=88917`.

Chattopadhyay, S., and McMechan, G. A., 2008, Imaging conditions for prestack reverse-time migration: GEOPHYSICS, **73**, No. 3, S81–S89.

Daley, T., Miller, D., Dodds, K., Cook, P., and Freifeld, B., 2016, Field testing of modular borehole monitoring with simultaneous distributed acoustic sensing and geophone vertical seismic profiles at Citronelle, Alabama: Geophysical Prospecting, **64**, No. 5, 1318–1334, `https://onlinelibrary.wiley.com/doi/pdf/10.1111/1365-2478.12324`.

Gordon, A. J., 2019, Processing of DAS and geophone VSP data from the CaMI Field Research Station: M.Sc. thesis, University of Calgary, `https://prism.ucalgary.ca/handle/1880/110175?`

Hartog, A. H., 2018, An introduction to distributed optical fibre sensors: CRC Press.

Lawton, D., Bertram, M., Hall, K., and Bertram, K., 2015, New approaches to seismic monitoring at the Brooks Field Research Station, Tech. rep., CREWES, `https://www.crewes.org/ForOurSponsors/ResearchReports/2015/CRR201541.pdf`.

Lawton, D., Bertram, M., Saeedfar, A., Macquet, M., Hall, K., Bertram, K., Innanen, K., and Isaac, H., 2017, DAS and seismic installations at the CaMI Field Research Station, Newell County, Alberta, Tech. rep., CREWES, `https://www.crewes.org/ForOurSponsors/ResearchReports/2017/CRR201751.pdf`.

Liang, W., Wu, X., Wang, Y., and Yang, C., 2018, A simplified staggered-grid finite-difference scheme and its linear solution for the first-order acoustic wave-equation modeling: Journal of Computational Physics, **374**, 863 – 872, `http://www.sciencedirect.com/science/article/pii/S0021999118305333`.

Macquet, M., Lawton, D. C., Saeedfar, A., and Osadetz, K. G., 2019, A feasibility study for detection thresholds of CO2 at shallow depths at the CaMI Field Research Station, Newell County, Alberta, Canada: Petroleum Geoscience, **25**, No. 4, 509–518, `https://pg.lyellcollection.org/content/25/4/509.full.pdf`.

Mateeva, A., Lopez, J., Mestayer, J., Wills, P., Cox, B., Kiyashchenko, D., Yang, Z., Berlang, W., Detomo, R., and Grandi, S., 2013, Distributed acoustic sensing for reservoir monitoring with vsp: The Leading Edge, **32**, No. 10, 1278–1283, `https://doi.org/10.1190/tle32101278.1`.
URL `https://doi.org/10.1190/tle32101278.1`

Wang, Y., Huang, L., and Zhang, Z., 2011, Reverse-time migration of time-lapse walkaway vsp data for monitoring co2 injection at the sacroc eor field, *in* SEG Technical Program Expanded Abstracts 2011, 4304–4308, `https://library.seg.org/doi/pdf/10.1190/1.3628107`.